Acta Pharmaceutica Sinica B 2026;16(2):820−835

Chinese Pharmaceutical Association
Institute of Materia Medica, Chinese Academy of Medical Sciences

Acta Pharmaceutica Sinica B

www.elsevier.com/locate/apsb
www.sciencedirect.com

ORIGINAL ARTICLE

OTUD6A drives dopaminergic neuronal degeneration of Parkinson's disease through deubiquitinating ACTG1 in neuronal cells

Xia Zhao[a,b], Fan Chen[a,b], Li Xiong[a], Xiaoxia Xu[a], Ziyao Meng[a], Yu Deng[b], Qi Ai[b], Luyao Li[c], Qin Yu[a], Linjie Chen[a], Ruya Wang[a], Yiyu Ren[a], Wenhua Zheng[d], Jurui Wei[b], Houming Yu[b], Guang Liang[a,b,c,*]

[a]*School of Pharmaceutical Sciences, Hangzhou Medical College, Hangzhou 311399, China*
[b]*The First People's Hospital of Lin'an District, Affiliated Lin'an People's Hospital, Hangzhou Medical College, Hangzhou 310014, China*
[c]*Chemical Biology Research Center, School of Pharmaceutical Sciences, Wenzhou Medical University, Wenzhou 325035, China*
[d]*Center of Reproduction, Development and Aging and Institute of Translation Medicine, Faculty of Health Sciences, University of Macau, Taipa 999078, China*

Received 24 June 2025; received in revised form 6 October 2025; accepted 15 October 2025

KEY WORDS

Parkinson's disease;
Deubiquitinating enzymes;
OTUD6A;
ACTG1;
p53;
Motor deficits;
Neurodegeneration;
Apoptosis

Abstract Parkinson's disease (PD) is a severe neurodegenerative disorder characterized by the progressive loss of dopaminergic neurons. Emerging evidence suggests that deubiquitinating enzymes (DUBs), which regulate protein homeostasis through the cleavage of ubiquitin chains, play critical roles in PD pathogenesis. In this study, we discovered that a DUB, ovarian tumor deubiquitinase 6A (OTUD6A), was significantly upregulated in both PD patients and PD mouse models. Notably, OTUD6A deficiency effectively protected dopaminergic neurons from degeneration and improved motor deficits in both acute and chronic PD mouse models. Through comprehensive mass spectrometry analysis and co-immunoprecipitation assays, we identified that actin gamma 1 (ACTG1) serves as a key substrate of OTUD6A. Mechanistically, OTUD6A specifically interacts with the 8−181 aa domain of ACTG1 and preferentially cleaves K48-linked polyubiquitin chains, thereby enhancing ACTG1 protein stability in neuronal cells. The stabilized ACTG1 subsequently binds to p53 and facilitates its nuclear translocation, leading to the transcriptional activation of pro-apoptotic genes and promoting neuronal apoptosis.

*Corresponding author.
E-mail address: liangguang@wmu.edu.cn (Guang Liang).

Peer review under the responsibility of Chinese Pharmaceutical Association and Institute of Materia Medica, Chinese Academy of Medical Sciences.

https://doi.org/10.1016/j.apsb.2025.12.002

Collectively, our findings demonstrate that OTUD6A promotes dopaminergic neuron degeneration and PD progression by deubiquitinating and stabilizing ACTG1, which in turn activates a p53-dependent apoptotic pathway. These findings identify OTUD6A as a potential therapeutic target for PD intervention.

1. Introduction

Parkinson's disease (PD) is a major neurodegenerative disorder that predominantly affects the aging population[1]. The characteristic clinical manifestations of PD include resting tremor, muscular rigidity, bradykinesia, and postural instability, which collectively lead to progressive motor impairment[2]. At the pathological level, PD is primarily characterized by the progressive degeneration of dopaminergic neurons in the substantia nigra pars compacta[3]. Current treatment strategies primarily rely on dopamine replacement therapy, which aims to restore dopaminergic transmission and alleviate motor symptoms[4]. Although this approach offers symptomatic benefit, it is limited by significant side effects, including gastrointestinal complaints, psychiatric complications, and sleep disturbances[3,5]. Moreover, the short half-life of dopaminergic agents and the progressive nature of the disease often lead to diminished therapeutic efficacy over time[6]. The loss of dopaminergic neurons remains a central pathological hallmark of PD[7]. However, the underlying molecular mechanisms are not fully elucidated. A deeper understanding of the pathways mediating dopaminergic neuronal injury is essential for identifying novel therapeutic targets and developing more effective treatments for PD.

Ubiquitination is a dynamic and reversible post-translational modification that plays a critical role in regulating protein stability, localization, and function, with profound implications for neurodegenerative disease pathogenesis[8-10]. Deubiquitinating enzymes (DUBs) serve as key counter-regulatory elements in this system, reversing ubiquitination by selectively cleaving ubiquitin chains from substrate proteins[11]. Growing evidence links dysregulated DUB activity to the onset and progression of neurological disorders[12,13]. For example, USP14 inhibits neuronal ferroptosis by deubiquitinating GPX4 following cerebral ischemia−reperfusion, whereas CYLD promotes oxidative stress-induced neuronal death through RIP1 deubiquitination[14,15]. USP8 regulates α-synuclein deubiquitination and homeostasis, thereby mitigating neurotoxicity[16]. USP30 reduces mitochondrial protein ubiquitination level, suppressing excessive reactive oxygen species (ROS) production and protecting neurons from oxidative damage in PD[17]. These findings collectively suggest the significance of DUBs in neuronal survival and death pathways, highlighting their potential as therapeutic targets in neurodegenerative conditions.

Through analysis of public RNA-seq data from PD patient brain tissues, we observed significant upregulation of ovarian tumor deubiquitinase 6A (OTUD6A). OTUD6A has been implicated in key cellular processes, including DNA damage response and apoptosis[18]. For instance, it promotes prostate cancer progression by deubiquitinating and stabilizing Brg1 and AR proteins[19], and facilitates DNA damage repair by regulating TopBP1 turnover[20]. Although these studies establish OTUD6A as a regulator of cell survival in cancer, its role in PD pathogenesis remains unknown.

In this study, we demonstrate that *Otud6a* deficiency attenuates dopaminergic neuron loss and motor deficits in both 6-OHDA-induced and A53T α-synuclein mouse models of PD. Mechanistically, OTUD6A binds to and stabilizes ACTG1 (actin gamma 1) through removal of K48-linked polyubiquitin chains, leading to enhanced nuclear translocation of p53 and activation of pro-apoptotic signaling in neurons. Our results identify OTUD6A as a critical contributor to PD pathogenesis and suggest its potential as a therapeutic target.

2. Materials and method

2.1. General reagents

Dulbecco's modified Eagle's medium (DMEM, D1152), dimethyl sulfoxide (DMSO, D2650), MTT (M2128), penicillin/streptomycin (RNBK9934), and bovine serum albumin (BSA, A1933) from Sigma−Aldrich (St. Louis, MO, USA); ROS assay kit (S0033S), JC-1 assay kit (C2006), and RIPA lysis buffer (P0013B) from Beyotime Institute of Biotechnology (Shanghai, China); Lipofectamine™ 8000 (L3000-015), BCA rapid protein quantification kit (A53225), Opti-MEM (31985070), and 0.25% trypsin (BC-CE-005) from Thermo Fisher Scientific (Sunnyvale, CA, USA); 6-hydroxydopamine (6-OHDA, S30042) from Shanghai Yuanye Bio-Technology Co., Ltd. (China); Annexin V-FITC/PI Apoptosis Detection Kit (556570) from BD Biosciences (San Diego, CA, USA); Western Blot Marker (C520010) from Sangon Biotech (Shanghai, China); PVDF membrane (1620177) from Bio-Rad (Shanghai, China); ECL Enhanced Chemiluminescent Substrate (P10300) from NCM Biotech (Suzhou, China); and Nuclear/Cytosol Fractionation Kit (P1200) from Applygen (Beijing, China). Antibodies, siRNA sequences, and AAV vector sources are provided in Supporting Information Tables S1, S2, and S3, respectively.

2.2. Brain stereotactic injection

Stereotaxic injections into the striatum were performed using coordinates derived from the Paxinos and Franklin mouse brain atlas (Paxinos & Franklin, 2001). The injection site was targeted at the following coordinates relative to bregma: anterior−posterior −1.0 mm from bregma, mediolateral ±0.5 mm from midline, and dorsoventral −2.5 mm from dura. Mice were anesthetized by intraperitoneal injection of 1% pentobarbital sodium (40 mg/kg). After full anesthesia was achieved, cranial hair was removed and the animal was positioned in a stereotaxic frame. A midline scalp incision was made to expose the skull, and bregma and lambda were identified. The microsyringe needle was positioned at bregma and the coordinates were zeroed. The needle was then moved to the predetermined striatal coordinates, and the injection site was marked on the skull. A burr hole was drilled at the marked

location, and the viral vector or vehicle (for sham-operated controls) was infused at a rate of 0.1 μL/min. The needle remained in place for an additional 5 min post-injection to minimize backflow before being slowly withdrawn. All procedures were conducted under aseptic conditions, and body temperature was maintained at 37 °C using a feedback-controlled heating pad.

2.3. Animal models and OTUD6A knockout PD mice

The A53T α-synuclein transgenic mice (B6-hSNCA-A53T, Strain No. T054329) were obtained from GemPharmatech (Nanjing, China). Whole-body *Otud6a* knockout mice (*Otud6a*$^{-/-}$) on a C57BL/6 background and wild-type C57BL/6 controls were generously provided by Wenzhou Medical University (Wenzhou, China). All animals were housed under specific pathogen-free conditions at the Hangzhou Medical College Animal Research Center, with environmental parameters maintained as follows: temperature: temperature 22 ± 2 °C, humidity 50%−60%, and a 12-h light/dark cycle. Standard rodent diet and water were provided *ad libitum*. The experimental protocol was approved by the Hangzhou Medical College Animal Ethics Committee (202502029, China).

2.3.1. 6-OHDA-induced acute PD model in Otud6a−/− mice

6-Hydroxydopamine (6-OHDA), a hydroxylated dopamine analog, is a selective catecholaminergic neurotoxin widely used to establish PD models. Unilateral striatal injection of 6-OHDA (10 ng) induces selective degeneration of dopaminergic neurons, leading to motor asymmetry that manifests as ipsilateral rotations. In this study, male *Otud6a*$^{-/-}$ and wild-type (WT) mice (8 weeks old, 22−24 g) were randomly assigned to four groups ($n = 10$ per group): WT + sham, WT + 6-OHDA, *Otud6a*$^{-/-}$ + sham, and *Otud6a*$^{-/-}$ + 6-OHDA.

2.3.2. AAV-mediated Otud6a knockdown in A53T transgenic mice

The A53T α-synuclein transgenic mouse is a well-established model that recapitulates key PD pathologies, including α-synuclein (α-Syn) and Lewy body formation. To investigate the role of OTUD6A in PD progression, we performed neuron-specific knockdown using an adeno-associated virus (AAV) system. The following vectors were co-injected at a 1:1 ratio into the striatum *via* stereotaxic surgery: AAV-sh*OTUD6A* (rAAV-U6-DIO-shRNA(*Otud6a*)-3′CMV-mCherry-PA) and AAV-Cre (rAAV-hSyn-CRE-WPRE-hGH polyA). Experimental groups included: WT + AAV-NC ($n = 10$); A53T + AAV-NC ($n = 10$); A53T + AAV-sh*Otud6a* ($n = 10$). All mice were male, 6 months of age (28−30 g). Behavioral tests were conducted 4 weeks post-injection to allow for sufficient transgene expression and phenotypic development.

2.4. Behavior tests

The open field test was used to assess spontaneous locomotor activity in mice, as previously described with minor modifications[21]. Briefly, each mouse was gently placed in the center of a square arena (40 cm × 40 cm × 40 cm) and allowed to explore freely for 5 min. Sessions were recorded using an automated video tracking system (EthoVision XT, Noldus). Total distance traveled and average speed were analyzed to evaluate general locomotor activity. Between trials, the arena was thoroughly cleaned with 75% ethanol to eliminate olfactory cues. All tests were conducted under consistent lighting and noise conditions.

The swimming test was conducted using a transparent cylindrical chamber (16 cm diameter × 28 cm height) filled with 5 L of water maintained at 25 ± 1 °C. Each mouse was gently placed into the water and allowed to swim freely for 5 min while being recorded for behavioral analysis. Immobility time was defined as the duration during which the mouse floated passively without active limb movement. After each trial, the mouse was promptly removed, dried gently, and placed under a heat lamp to avoid hypothermia. The tank was thoroughly cleaned and refilled with fresh water between trials to maintain consistent testing conditions.

2.5. Cell transfection

PC12 cells or primary culture dopaminergic neurons were seeded into 6-well plates at a density of 1×10^5 cells per well and cultured for 24 h to reach 70%−80% confluence prior to transfection. Transfection was performed using Lipofectamine™ 8000 according to the manufacturer's protocol. Briefly, plasmid DNA or siRNA was diluted in Opti-MEM medium and gently mixed with an equal volume of Lipofectamine™ 8000 diluted in Opti-MEM. The mixture was incubated at room temperature for 20 min to allow complex formation, then added dropwise to the cells. After 6 h of incubation, the medium was replaced with fresh complete medium. The following experimental groups were established: NC siRNA: transfected with negative control siRNA; si*Otud6a*: transfected with *Otud6a*-targeting siRNA; NC-OE: transfected with empty vector, OE-*Otud6a*: transfected with *Otud6a* overexpression plasmid; and si*Actg1*+ OE-*Otud6a*: transfected with OE-*Otud6a* for 24 h, followed by *ACTG1* siRNA for an additional 24 h. Cells were harvested 24 h post-transfection for subsequent analyses.

2.6. Nuclear−cytosol extraction

Nuclear and cytosolic protein extracts were prepared using a commercial fractionation kit according to the manufacturer's instructions. Following treatment, PC12 cells were washed twice with ice-cold PBS and harvested by scraping in Cytosol Extraction Buffer-A (CEB-A; 100 μL per 1×10^6 cells). The cell suspension was transferred to a pre-chilled 1.5 mL tube, vortexed vigorously for 30 s, and incubated on ice for 15 min with intermittent vortexing every 5 min. Subsequently, 1/20 volume of CEB-B was added, followed by brief vortexing and incubation on ice for 1 min. The lysate was centrifuged at 1000×*g* for 5 min at 4 °C. The supernatant (cytosolic fraction) was collected and further clarified by centrifugation at 12,000×*g* for 10 min at 4 °C. The crude nuclear pellet was washed twice with a mixture of CEB-A and CEB-B (100 μL + 5 μL), followed by centrifugation at 1000×*g* for 5 min. The washed pellet was resuspended in 100 μL of pre-cooled Nuclear Extraction Buffer (NEB), vortexed vigorously for 15 s, and incubated on ice for 30 min with vortexing every 10 min. The nuclear extract was then centrifuged at 12,000×*g* for 5 min at 4 °C, and the resulting supernatant was collected as the nuclear protein fraction. All extracts were aliquoted and stored at −80 °C until use.

2.7. Isolation and culture of primary ventral mesencephalic neurons

Primary ventral mesencephalic (VM) cultures were prepared from P0 C57BL/6 mouse (born within 24 h) following an established protocol with minor modifications[22]. Briefly, VM tissues were

dissected, trypsinized for 5 min at 37 °C, and gently triturated to obtain a single-cell suspension. The suspension was filtered through a 70 μm cell strainer and centrifuged at 200×*g* for 5 min at 4 °C. The pellet was resuspended in Neurobasal Medium supplemented with 1% B27 and plated on poly-D-lysine-coated culture vessels. Cultures were maintained in a humidified incubator at 37 °C with 5% CO_2.

2.8. Bioinformatic analysis of GEO datasets

Publicly available transcriptomic datasets related to PD were retrieved from the Gene Expression Omnibus (GEO) database (https://www.ncbi.nlm.nih.gov/geo/) using the search term "Parkinson's disease". Datasets containing both PD patient-derived samples and healthy controls were selected for further analysis. Raw data files (CEL format) were downloaded and processed using the affy package in R/Bioconductor. Background correction and quantile normalization were performed using the Robust Multi-Array Average (RMA) algorithm to generate standardized gene expression matrices. The normalized expression value of OTUD6A was extracted from each dataset. Differential expression analysis between PD and control samples was conducted using the limma package, with significance thresholds set at $|\log_2$ fold change$| > 0.5$ and adjusted *P*-value <0.05.

2.9. Identification of OTUD6A-interacting proteins by LC−MS/MS

To identify potential substrates of OTUD6A, liquid chromatography−tandem mass spectrometry (LC−MS/MS) was employed. NIH3T3 cells were transiently transfected with either a Flag-tagged OTUD6A plasmid or an empty Flag vector (control) for 24 h. Cells were lysed in RIPA buffer supplemented with protease inhibitors, and protein concentration was determined using a BCA assay. Flag-tagged proteins and associated complexes were immunoprecipitated using anti-Flag magnetic beads under stringent washing conditions (three washes with high-salt buffer). Immunoprecipitated proteins were eluted, reduced with 10 mmol/L DTT, alkylated with 50 mmol/L iodoacetamide, and digested overnight with sequencing-grade trypsin at 37 °C. The resulting peptides were desalted using C18 StageTips and separated on a reversed-phase C18 column with a 90 min gradient of 5%−35% acetonitrile in 0.1% formic acid. MS analysis was performed on an Orbitrap Fusion Lumos mass spectrometer operated in data-dependent acquisition mode, with full MS scans at 120,000 resolution and MS/MS scans for the top 20 most intense ions. Raw data were processed using MaxQuant (v2.0.3) and searched against the UniProt *Mus musculus* database with a false discovery rate (FDR) set to 1%. Proteins enriched in Flag-OTUD6A samples compared to the Flag-control, with at least two unique peptides and a fold change >2, were considered high-confidence OTUD6A interactors. All experiments were performed in three biological replicates to ensure reproducibility of the results.

2.10. Immunofluorescence staining and analysis

Brain tissues from each experimental group were perfusion-fixed with 4% paraformaldehyde (PFA), post-fixed by immersion in the same fixative for 24 h at 4 °C, and cryoprotected by sequential incubation in 20% and 30% sucrose solutions until the tissues sank. After embedding in optimal cutting temperature (OCT) compound, coronal sections were cut at a thickness of 20 μm using a cryostat (Leica CM1950). For immunofluorescence staining, sections were washed in PBS, permeabilized with 0.3% Triton X-100 for 10 min, and blocked with 10% bovine serum albumin (BSA) in PBS for 1 h at room temperature. Sections were then incubated with primary antibodies (diluted in blocking solution) overnight at 4 °C. After three washes with PBS, species-matched Alexa Fluor-conjugated secondary antibodies were applied for 2 h at room temperature in the dark. Nuclei were stained with DAPI (1 μg/mL) for 5 min. Finally, sections were mounted with antifade mounting medium and imaged using a confocal microscope (Zeiss LSM 880). Fluorescence intensity and positive cell counts were quantified in defined regions of interest using Image J software (NIH). Three sections per animal and at least three randomly selected fields per section were analyzed for each marker.

2.11. Co-immunoprecipitation and Western blot analysis

After treatment, cells were washed twice with ice-cold PBS and lysed in RIPA buffer containing protease and phosphatase inhibitors on ice for 30 min. Lysates were centrifuged at 12,000×*g* for 15 min at 4 °C, and supernatants were collected for protein quantification using a BCA assay. For co-immunoprecipitation (Co-IP), equal amounts of protein (500−1000 μg) were incubated with 2−5 μg of the indicated primary antibody overnight at 4 °C with gentle rotation. Protein A/G magnetic beads were pre-blocked with 5% BSA and added to the lysate-antibody mixture for 2 h at 4 °C. Beads were then washed four times with lysis buffer, and bound proteins were eluted by boiling in 2 × Laemmli sample buffer for 10 min. For Western blotting, proteins were separated by SDS-PAGE and transferred to PVDF membranes. After blocking with 5% non-fat milk for 1 h, membranes were incubated with primary antibodies overnight at 4 °C, followed by HRP-conjugated secondary antibodies for 1 h at room temperature. Signals were detected using an ECL substrate and imaged with a ChemiDoc system. Where indicated, inputs (whole-cell lysates) and Co-IP eluates were analyzed in parallel to confirm specific interactions.

2.12. Statistical analysis

All quantitative data are expressed as mean ± standard deviation (SD) (or SEM where appropriate), as indicated in the figure legends. Statistical analyses were performed using GraphPad Prism software (version 8.0). Differences between two groups were evaluated using an unpaired two-tailed Student's *t*-test. For comparisons among three or more groups, one-way analysis of variance (ANOVA) was applied, followed by Tukey's *post hoc* test for multiple comparisons. The threshold for statistical significance was uniformly set to $P < 0.05$ for all analyses. In figures, statistical significance was denoted using standard conventions: $P < 0.05$, with non-significant differences ($P \geq 0.05$) labeled as "ns" to avoid ambiguity. All experimental data were derived from biological replicates ($n \geq 3$) and technical duplicates to ensure reproducibility.

3. Results

3.1. Otud6a expression is upregulated in PD models

Bioinformatic analysis of publicly available transcriptomic data revealed a significant increase in *OTUD6A* expression in PD

patients compared to healthy controls (Fig. 1A and B). To experimentally validate this finding, we established an acute PD model by unilateral striatal injection of 6-hydroxydopamine (6-OHDA) in mice (Fig. 1C). Consistent with the human data, both qPCR and Western blot analyses showed a marked upregulation of *OTUD6A* mRNA and protein levels in the substantia nigra of 6-OHDA-treated mice relative to sham controls (Fig. 1D−F). This increase was further confirmed in A53T α-synuclein transgenic mice, a chronic PD model (Fig. 1G and H). Immunofluorescence staining combined with neural cell markers indicated that OTUD6A was predominantly expressed in tyrosine hydroxylase-positive (TH^+) dopaminergic neurons, with minimal expression in $Iba1^+$ microglia or $GFAP^+$ astrocytes (Fig. 1I). TH, a pathological hallmark of PD, is one of the key enzymes of dopamine synthesis in the human body[23]. Consistent with this cellular specificity, IF analysis revealed a pronounced increase in OTUD6A expression within TH^+ neurons in the substantia nigra of both 6-OHDA-lesioned and A53T transgenic mice (Supporting Information Fig. S1). *In vitro* studies in PC12 cells further supported these observations, demonstrating that 6-OHDA treatment induced OTUD6A upregulation in a dose- and time-dependent manner (Fig. 1J−M). Together, these results indicate that OTUD6A expression is elevated across multiple PD models and is primarily localized to vulnerable dopaminergic neurons, suggesting a potential role in PD pathogenesis.

3.2. *Otud6a deficiency attenuates 6-OHDA induced PC12 cell apoptosis*

To examine the functional role of OTUD6A in 6-OHDA induced neurotoxicity, PC12 cells were transfected with OTUD6A specific siRNA (si*Otud6a*) followed by 24 h exposure to 6-OHDA. Flow cytometry analysis indicated that silencing *OTUD6A* markedly suppressed 6-OHDA-induced apoptosis (Fig. 2A and B). MTT assays showed that 6-OHDA significantly reduced cell viability, and this reduction was improved by *Otud6a* knockdown (Fig. 2C). Western blot results further demonstrated that OTUD6A depletion increased the level of the anti-apoptotic protein Bcl2, decreased the pro-apoptotic protein Bax, and inhibited caspase-3 activation (Fig. 2D and E). In contrast, overexpression of *Otud6a* exacerbated 6-OHDA triggered neuronal injury in PC12 cells (Fig. 2F−J). These data collectively indicate that OTUD6A promotes apoptotic signaling and contributes to 6-OHDA induced neurotoxicity in neuronal cells.

3.3. *Neuronal knockdown of Otud6a ameliorates motor deficits and dopaminergic degeneration in A53T mice*

To evaluate the pathological contribution of OTUD6A in PD, we performed stereotaxic injection of AAV-sh*Otud6a* into the striatum of A53T α-synuclein transgenic mice to achieve neuron-specific knockdown of *OTUD6A*, the efficiency of which was confirmed by Western blot (Supporting Information Fig. S2). Four weeks post-injection, a series of behavioral tests were conducted, including the swimming test, open field test, and pole test (Fig. 3A). In the swimming test (Fig. 3B), A53T mice showed significant motor impairment, characterized by decreased total movement distance (Fig. 3C) and reduced swimming speed (Fig. 3D) compared to wild-type controls. These deficits were markedly rescued by *Otud6a* knockdown. The open field test (Fig. 3E) further revealed that *Otud6a*-deficient mice exhibited increased total distance traveled (Fig. 3F) and average speed (Fig. 3G), along with greater central zone exploration time (Fig. 3H) and distance (Fig. 3I), indicating enhanced locomotor activity and reduced anxiety-like behavior. Moreover, in the pole test, *Otud6a* knockdown significantly improved motor coordination, as evidenced by shortened descent time (Fig. 3J and K). Collectively, these behavioral data demonstrate that neuronal *Otud6a* knockdown alleviates motor dysfunction in A53T transgenic mice.

We next assessed whether OTUD6A inactivation protected dopaminergic neurons in the substantia nigra. Immunofluorescence staining showed a significant reduction in TH-positive neurons and P-Syn-positive neurons in A53T mice compared to wild-type controls, which was effectively restored by *Otud6a* knockdown (Fig. 3L−O). Western Blot further confirmed the results (Fig. 3P−R). The TUNEL apoptosis assay further confirmed that *Otud6a* knockdown significantly reduced neuronal apoptosis in the substantia nigra of A53T mice (Supporting Information Fig. S3). At the molecular level, *Otud6a* knockdown increased the expression of the anti-apoptotic protein Bcl2, while decreasing levels of the pro-apoptotic protein Bax and cleaved caspase-3 (Fig. 3S−U). These results indicate that *Otud6a* deficiency exerts neuroprotective effects by preserving dopaminergic neuronal survival and inhibiting apoptotic signaling in a genetic PD model.

3.4. *Otud6a deficiency protects against motor impairment and dopaminergic degeneration in a 6-OHDA induced PD model*

To further assess the role of OTUD6A in an acute PD model, we performed unilateral striatal injection of 6-OHDA (10 ng/mouse) in age- and sex-matched wild-type and *Otud6a* knockout ($Otud6a^{-/-}$) mice (Fig. 4A and Supporting Information Fig. S4). Swimming test analyses showed that 6-OHDA administration significantly impaired motor function (Fig. 4B), as reflected by decreased swimming speed (Fig. 4C) and total swimming distance (Fig. 4D). These deficits were markedly alleviated in $Otud6a^{-/-}$ mice. In the open field test (Fig. 4E), *Otud6a* knockout animals displayed improved exploratory behavior, with increased central zone duration (Fig. 4F) and movement distance (Fig. 4G) compared to 6-OHDA treated WT mice. Immunofluorescence staining of substantia nigra sections revealed that *Otud6a* deficiency significantly increased the TH-positive neurons and attenuated P-syn positive neurons induced by 6-OHDA (Fig. 4H−K), and concurrently reduced neuronal apoptosis (Fig. 4L and M). At the molecular level, *Otud6a* knockout counteracted 6-OHDA triggered activation of apoptotic pathways, decreasing pro-apoptotic Bax and cleaved caspase-3 levels while increasing anti-apoptotic Bcl2 expression in brain tissues (Fig. 4N−Q). Together, these results demonstrate that *Otud6a* deficiency exerts a protective effect in the 6-OHDA induced PD model by preserving motor function, maintaining dopaminergic neuron survival, and suppressing apoptosis-related signaling.

3.5. *OTUD6A interacts with and stabilizes ACTG1 via K48-linked deubiquitination*

To elucidate the molecular mechanism by which OTUD6A contributes to PD pathology, we performed LC−MS/MS and Co-IP assays to identify OTUD6A-interacting proteins. Both mass spectrometry (Fig. 5A and B) and subsequent Co-IP validation (Fig. 5C and D) identified γ-actin (ACTG1) as a direct binding partner of OTUD6A. identified γ-actin (ACTG1) as a specific OTUD6A binding partner. ACTG1 is a cytoskeletal protein previously

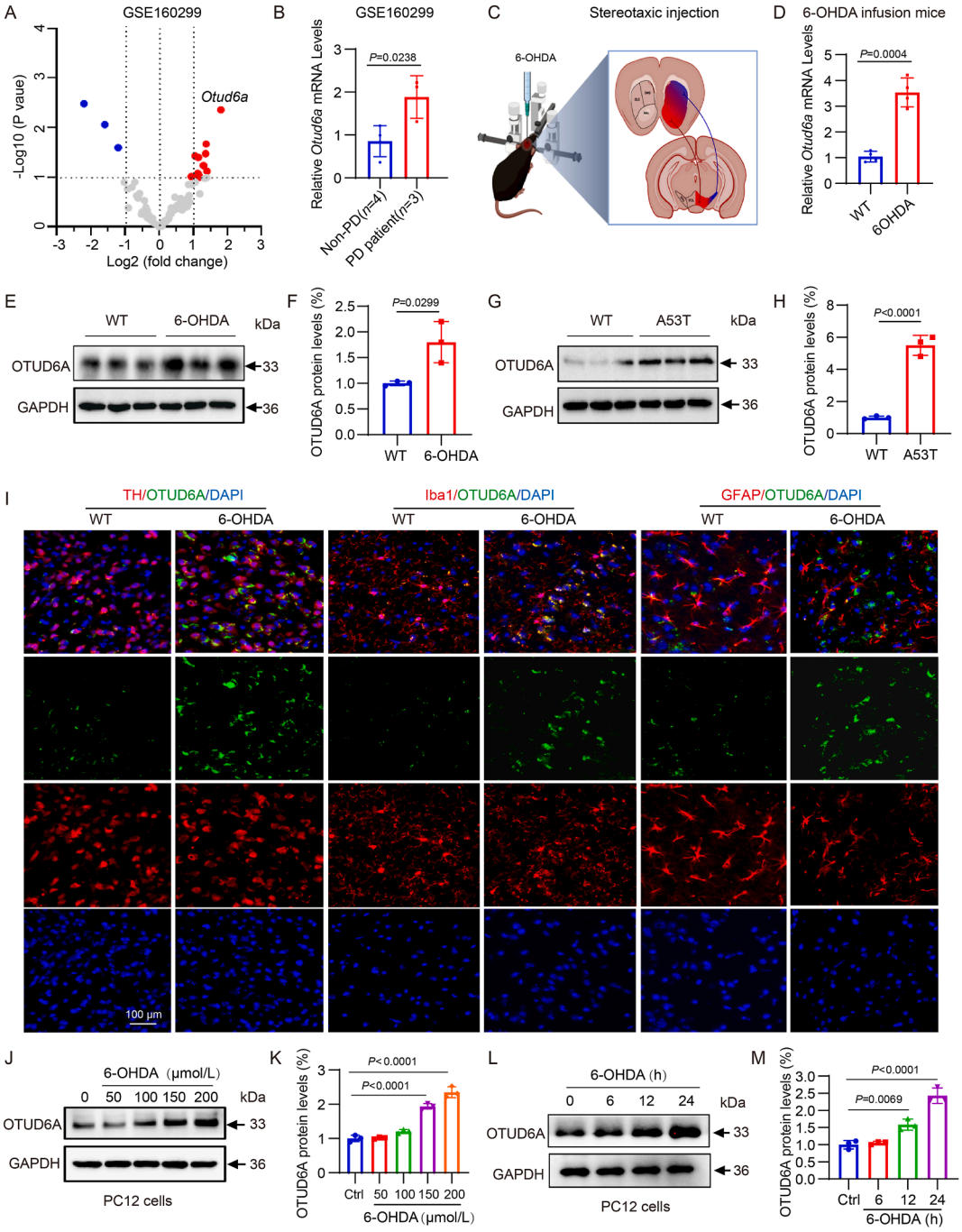

Figure 1 OTUD6A expression is upregulated in PD models. (A) Volcano plot depicting differentially expressed DUBs in postmortem brain tissues from PD patients and healthy controls (GSE160299 dataset). Red dots represent significantly upregulated DUBs ($P < 0.05$). (B) *OTUD6A* mRNA expression in PD patients compared to controls in the GSE160299 dataset. (C, D) qRT-PCR analysis of *Otud6a* mRNA levels in the substantia nigra of C57BL/6 mice after unilateral intrastriatal 6-OHDA injection *versus* wild-type (WT) controls. (E, F) Representative Western blot and quantitative analysis of OTUD6A protein expression in the 6-OHDA-induced PD mice model. (G, H) Expression of OTUD6A in WT and A53T α-synuclein transgenic mice. (I) Immunofluorescence analysis of OTUD6A (Green) expression in dopaminergic neurons (TH^+; Red), astrocytes ($GFAP^+$; Red), and microglia ($Iba1^+$; Red) (Green). (J) OTUD6A protein expression in PC12 cells treated with increasing concentrations of 6-OHDA. (K) Quantification of OTUD6A levels from (J). (L) OTUD6A expression in PC12 cells exposed to 6-OHDA for different durations. (M) Quantification of OTUD6A levels from (L). (Mean ± SEM; $n = 3$ independent experiments).

linked to apoptotic signaling and 6-OHDA induced dopaminergic degeneration[24-26]. These findings suggest that OTUD6A may exert its effects in PD pathogenesis through regulating ACTG1. To map the interaction domain, we generated a series of ACTG1 truncation mutants (Fig. 5E) and found that deletion of the N-terminal region (amino acids 8−181, Mut1) abolished binding to OTUD6A (Fig. 5F), indicating this region is essential for the interaction. We next examined the functional relationship between OTUD6A

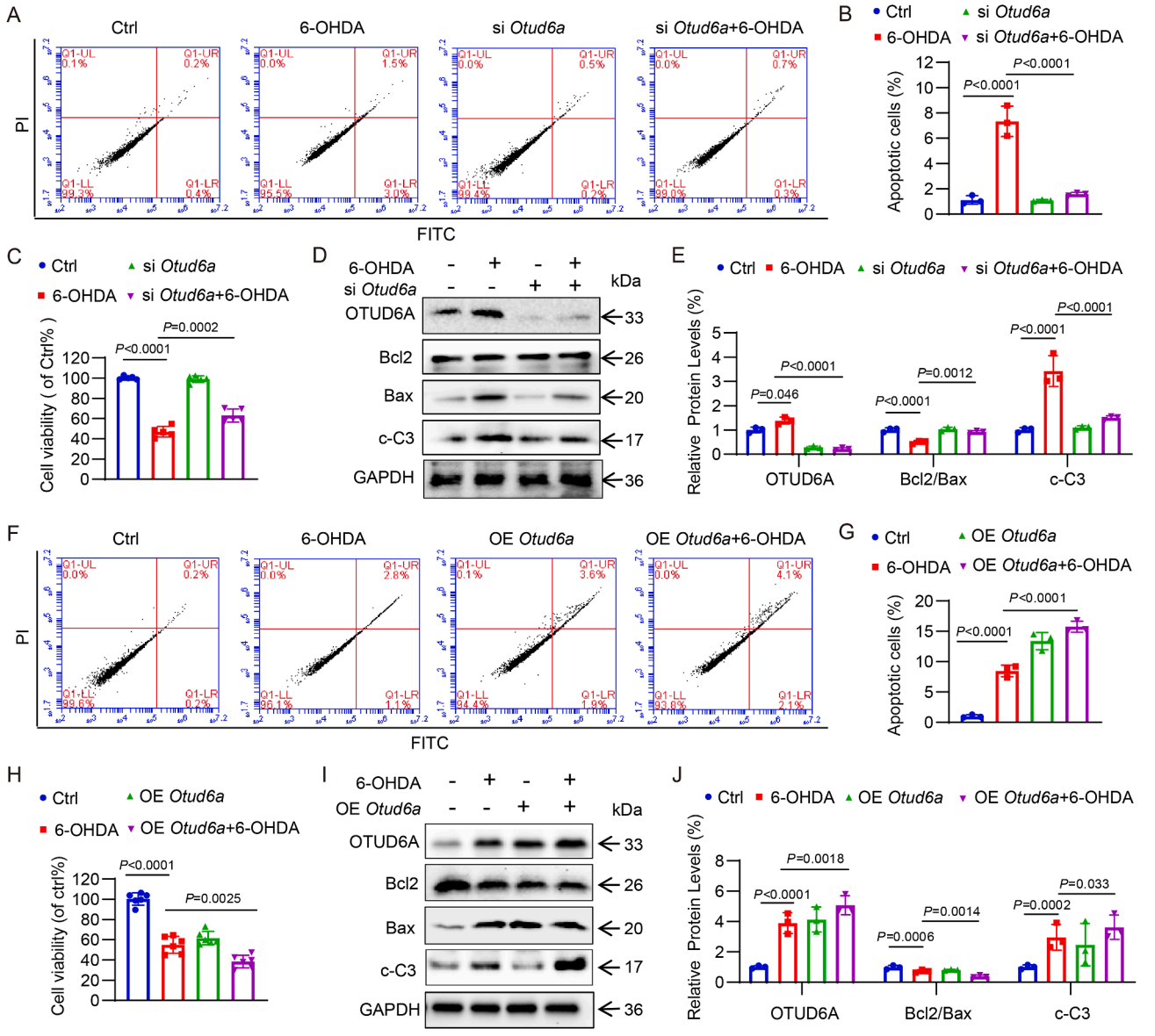

Figure 2 *Otud6a* knockdown attenuates 6-OHDA induced PC12 cells apoptosis. (A) Representative flow cytometry plots of apoptosis assessed by Annexin V-FITC/PI double staining under indicated treatments. (B) Quantification of apoptotic rates from A. (C) Cell viability measured by MTT assay in PC12 cells transfected with OTUD6A siRNA (si*Otud6a*) for 24 h and treated with 6-OHDA (100 μmol/L, 24 h) (Mean ± SEM; $n = 5$ duplicates/group). (D) Western blot analysis of OTUD6A, Bcl2, Bax, and cleaved caspase-3 expression in si*OTUD6A*-transfected cells. (E) Quantification of protein levels from (D). (F) Apoptosis analysis by flow cytometry in *OTUD6A*-overexpressing cells. (G) Quantification of apoptotic rates from (F). (H) MTT assay showing cell viability in PC12 cells overexpressing *Otud6a* (24 h transfection) followed by 6-OHDA treatment (24 h) (Mean ± SEM; $n = 6$ duplicates/group). (I) Western blot detection of apoptosis-related proteins in *Otud6a*-overexpressing cells. (J) Quantification of protein levels from (I). (Mean ± SEM; $n = 3$ independent experiments).

and ACTG1. In nigral neurons of PD model mice, OTUD6A and ACTG1 protein levels showed a strong positive correlation (Supporting Information Fig. S5A and S5B), which was further confirmed in *Otud6a* overexpressing PC12 cells (Fig. S5C and S5D). Cycloheximide chase assays revealed that *Otud6a* overexpression extended ACTG1 half-life (Fig. 5G), while *Otud6a* knockout accelerated its degradation (Fig. 5H). The proteasome inhibitor MG132, but not the autophagy inhibitor chloroquine (CQ), restored ACTG1 levels in *Otud6a* deficient cells (Fig. 5I and J), indicating that OTUD6A stabilizes ACTG1 primarily by inhibiting proteasomal degradation.

To determine the ubiquitination mechanism involved, we performed ubiquitination assays in PC12 cells expressing Flag-OTUD6A, His-ACTG1, and HA-ubiquitin. *Otud6a* overexpression markedly reduced ACTG1 ubiquitination (Fig. 5K), whereas *Otud6a* knockdown increased polyubiquitination (Fig. 5L). Further analysis showed that OTUD6A preferentially cleaved K48-linked ubiquitin chains from ACTG1 (Fig. 5M), and this activity was abolished when a K48R ubiquitin mutant was used (Fig. 5N). These results demonstrate that OTUD6A binds to and stabilizes ACTG1 by selectively removing K48-linked polyubiquitin chains, thereby antagonizing its proteasomal degradation.

3.6. *Otud6a deficiency attenuates 6-OHDA-induced apoptosis via the ACTG1−p53 signaling pathway*

To determine whether ACTG1 is required for OTUD6A mediated neuronal apoptosis, we performed genetic rescue experiments in PC12 cells by co-transfecting an *Otud6a* overexpression plasmid with *ACTG1* siRNA (Fig. 6A and B). The MTT assay revealed that *Otud6a* overexpression significantly reduced cell viability, an effect that was attenuated by concurrent *Actg1* knockdown (Fig. 6C). Western blot analysis further showed that *Otud6a*

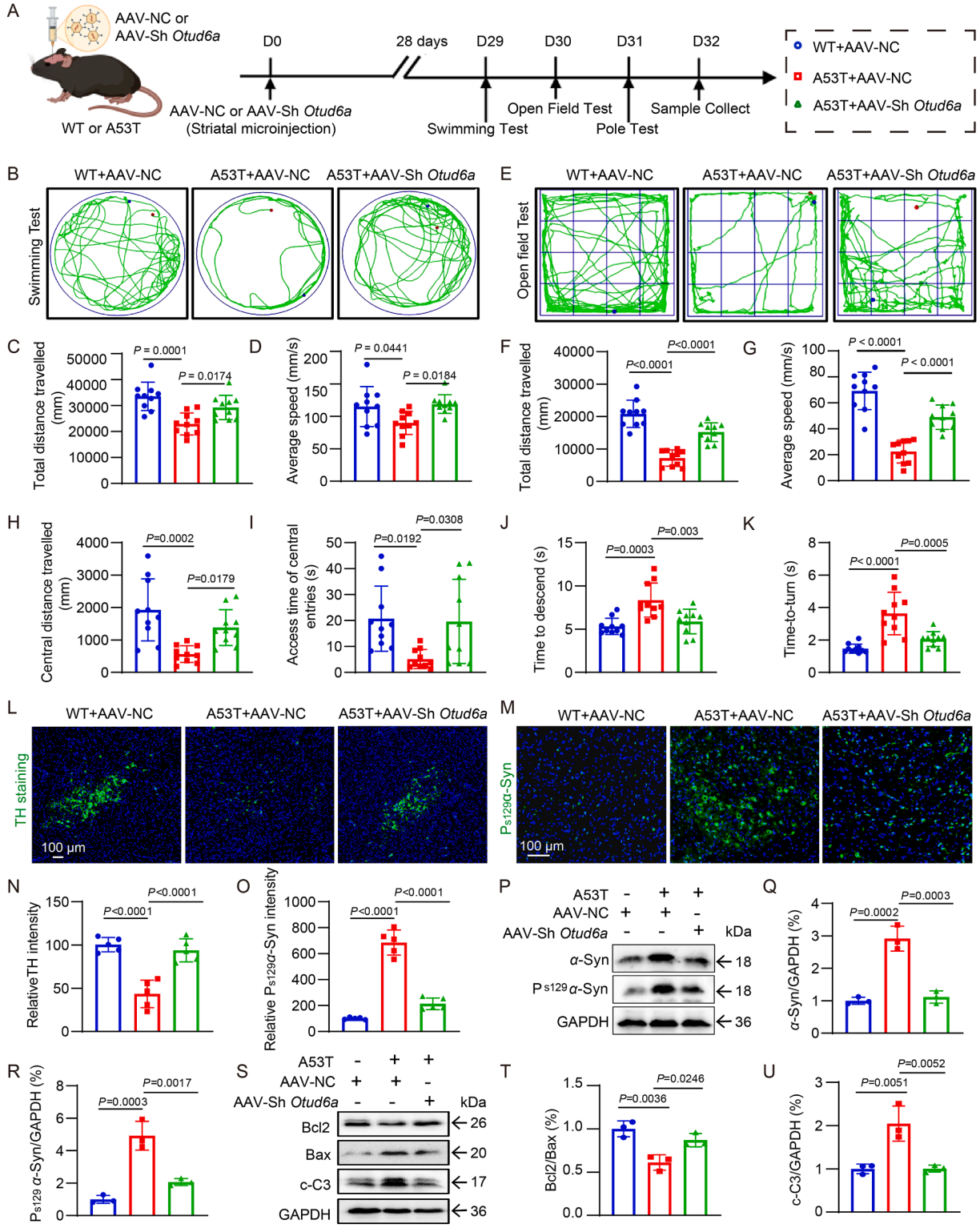

overexpression decreased Bcl2 expression and increased levels of Bax and cleaved caspase-3 (Fig. 6D and E). These pro-apoptotic effects were abolished when *Actg1* was silenced. Consistent with these results, flow cytometry analysis of apoptosis rates (Fig. 6F and G) and TUNEL staining (Fig. 6H and I) confirmed that *Actg1* knockdown blocked OTUD6A induced apoptosis. Furthermore, *Otud6a* knockdown reduced the mRNA level of *Bax*, whereas *Otud6a* overexpression further elevated the 6-OHDA-induced *Bax* mRNA expression (Supporting Information Fig. S6). Together, these findings establish ACTG1 as an essential downstream mediator of OTUD6A dependent apoptotic signaling in neuronal cells.

To identify downstream effectors of the OTUD6A−ACTG1 axis, we performed Co-IP coupled with LC−MS/MS in PC12 cells expressing Flag-ACTG1, which identified p53 as a key interacting protein (Fig. 7A and B). This finding is particularly significant given that p53 is a tumor suppressor[27] and mediates 6-OHDA-induced neuronal apoptosis[28,29]. Given the established role of p53 in 6-OHDA induced neuronal apoptosis, we validated this interaction by Co-immunoprecipitation (Fig. 7C) and molecular docking analysis (Fig. 7D and Supporting Information Table S4). Functionally, *Otud6a* knockdown attenuated 6-OHDA induced p53 upregulation, while *Otud6a* overexpression enhanced p53 expression (Fig. 7E and F). Immunofluorescence and subcellular fractionation assays further showed that 6-OHDA promoted nuclear accumulation of p53, an effect suppressed by *Otud6a* knockdown (Fig. 7G and H). Moreover, *Actg1* silencing abolished OTUD6A mediated p53 nuclear translocation (Fig. 7I), confirming that p53 acts downstream of ACTG1. Together, these data demonstrate that OTUD6A promotes dopaminergic neuron apoptosis through a linear signaling pathway involving ACTG1 stabilization and subsequent p53 activation and nuclear translocation.

3.7. Otud6a deficiency attenuates 6-OHDA-induced primary dopaminergic neuron apoptosis via the ACTG1−p53 signaling pathway

To further validate the regulatory role of the OTUD6A−ACTG1 axis in dopamine neuron apoptosis in PD, we isolated and cultured primary midbrain dopamine neurons from mice (Fig. 8A). Neuronal morphology was confirmed by microscopy, as shown in Fig. 8B. Immunocytochemistry (ICC) using an antibody against tyrosine hydroxylase (TH), a marker for dopamine neurons, indicated that more than 90% of the cultured cells were TH-positive following *Otud6a* knockdown (Fig. 8B and C). MTT assays demonstrated that knockdown of *Otud6a* significantly attenuated the 6-OHDA induced reduction in cell viability (Fig. 8D). Western blot analysis further indicated that *Otud6a* knockdown upregulated the anti-apoptotic protein Bcl2, downregulated the pro-apoptotic protein Bax, and suppressed caspase-3 activation (Fig. 8E and F). To investigate whether the ACTG1−p53 pathway contributes to OTUD6A-mediated effects, we performed ICC staining. Consistent with the findings in PC12 cells, *Otud6a* overexpression markedly increased the expression levels of p53 and Bax, whereas *Actg1* knockdown resulted in reduced expression of downstream proteins p53 and Bax induced by *Otud6a* overexpression (Fig. 8G−I). Taken together, these findings indicate that *Otud6a* deficiency protects against 6-OHDA-induced dopamine neuron damage *via* the ACTG1−p53 signaling axis.

4. Discussion

In this study, we demonstrated that OTUD6A is significantly upregulated in multiple PD models. Functional studies revealed that neuronal *Otud6a* knockdown or whole-body *Otud6a* knockout alleviated motor deficits and protected dopaminergic neurons damage. Mechanistically, OTUD6A promoted neuronal apoptosis by selectively removing K48-linked ubiquitin chains from ACTG1, thereby enhancing its stability. The accumulated ACTG1 facilitated p53 nuclear translocation, triggering a pro-apoptotic cascade that contributes to neurodegeneration in PD. Our findings reveal a previously unrecognized OTUD6A−ACTG1−p53 signaling axis and suggest OTUD6A as a potential therapeutic target for neuroprotective strategies in PD.

The ubiquitin−proteasome system, particularly deubiquitinating enzymes (DUBs), has emerged as a critical regulator of PD pathogenesis[30]. Several DUBs have been implicated in specific PD-related pathways. For example, USP30 negatively regulates PINK1/Parkin-mediated mitophagy, contributing to impaired mitochondrial quality control in SH-SY5Y cells[31], while OTUD3 promotes iron accumulation in the substantia nigra by stabilizing iron regulatory protein 2 (IRP2)[32]. In the present study, we identify OTUD6A as a novel PD-associated DUB that ameliorates motor deficits and neuronal apoptosis in experimental models. OTUD6A has previously been shown to regulate apoptotic pathways in cancer and inflammatory diseases[18]. For example, OTUD6A promotes breast cancer growth by boosting TopBP1 stability and making tumor cells resistant to DNA-damaging therapies[33]. OTUD6A promotes myocardial inflammation and hypertrophy *via* deubiquitinating STING in cardiomyocytes[34]. Our findings extend the functional relevance of OTUD6A to neurodegenerative disease and highlight its role in PD through the stabilization of ACTG1 and subsequent activation of p53-mediated apoptosis.

DUBs exert pleiotropic effects through substrate-specific deubiquitination[35,36]. Here, we demonstrate that OTUD6A

Figure 3 Knockdown of *Otud6a* ameliorates motor deficits and dopaminergic degeneration in A53T α-synuclein transgenic mice. (A) Experimental timeline and treatment scheme ($n = 10$ mice/group). (B) Representative swimming trajectories of mice from each group. (C) Total distance traveled in the swimming test. (D) Mean swimming speed during the swimming test. (E) Representative movement traces in the open field test. (F) Total travel distance in the open field test. (G) Average movement speed in the open field test. (H) Distance traveled in the center zone of the open field. (I) Time spent by mice in the central area of the open field experiment. (J) Time spent by mice climbing to the bottom in the pole test. (K) Time spent by mice turning around in the pole test. (L) Immunofluorescence staining of TH (green) in the substantia nigra of mice from each group. (M) Immunofluorescence staining of P^{S129}α-Syn (green) in the substantia nigra of mice from each group. (N) Quantification of TH fluorescence intensity. (O) Quantification of P^{S129}α-synuclein fluorescence intensity in each experimental group. (P) Western blot detection of α-Syn and P^{S129}α-Syn protein levels. (Q) Quantification of α-Syn levels from (P). (R) Quantification of P^{S129}α-Syn from (P). (S) Western blot analysis of Bcl2, Bax, and cleaved caspase3. (T) Quantification of Bcl2/Bax from (S). (U) Quantification of cleaved-caspase 3 from (S). (Mean ± SEM; $n = 3$ independent experiments).

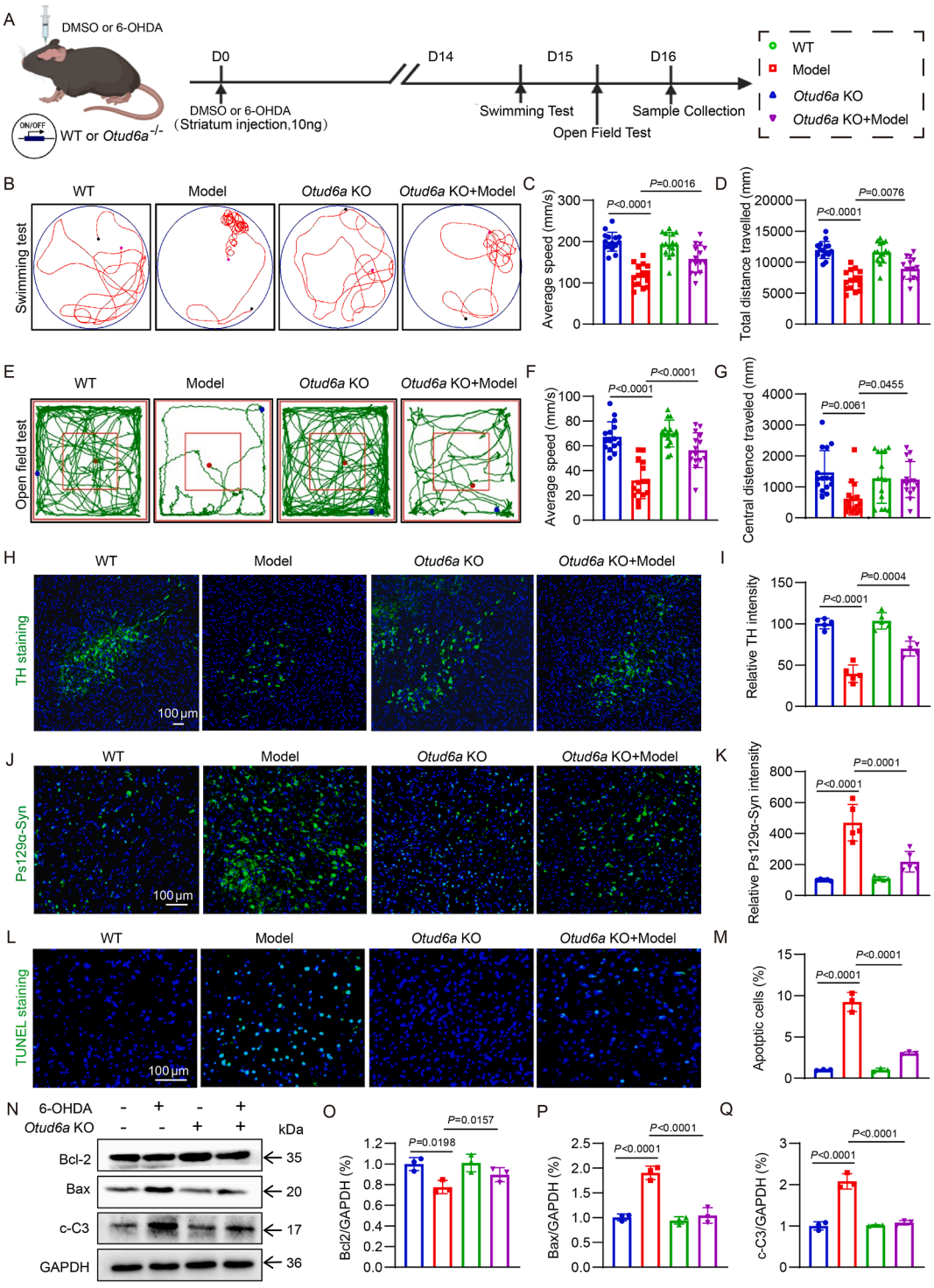

Figure 4 *Otud6a* deficiency protects against motor impairment and dopaminergic degeneration in a 6-OHDA-induced PD mouse model. (A) Schematic of the 6-OHDA-induced PD model and experimental timeline ($n = 10$ mice/group). (B) Representative swimming trajectories of mice from each group. (C) Average movement speeds of mice in each group during the swimming test. (D) Total distance traveled by mice in each group during the swimming test. (E) Representative mouse trajectories in open field tests. (F) Average movement speed of mice in the open field test. (G) Total distance traveled by mice in the open field test. (H) Immunofluorescence staining of TH (green) in the substantia nigra. (I) Quantification of TH fluorescence intensity. (J) Immunofluorescence staining of $P^{S129}\alpha$-Syn (green) in the substantia nigra of mice. (K) Quantification of $P^{S129}\alpha$-Syn fluorescence intensity. (L) TUNEL staining (green) of apoptotic cells in the substantia nigra. (M) Quantification of TUNEL positive cells. (N) Western Blot analysis of Bcl2, Bax, and cleaved-caspase3 expression. (O) Quantification of Bcl2 from (M). (P) Quantification of Bax from (L). (Q) Quantification of cleaved-caspase 3 from (M). (Mean ± SEM; $n = 3$ independent experiments).

directly interacts with and stabilizes ACTG1, a cytoskeletal protein with established roles in apoptosis regulation. Although primarily known for maintaining structural integrity and cellular motility, ACTG1 has been increasingly implicated in pathological processes[37]. In hepatocellular carcinoma, ACTG1 promotes tumor progression by modulating cell cycle activity and suppressing mitochondrial apoptosis, whereas its loss impairs proliferation in glioblastoma[38-40]. In PD models, ACTG1 has been reported to

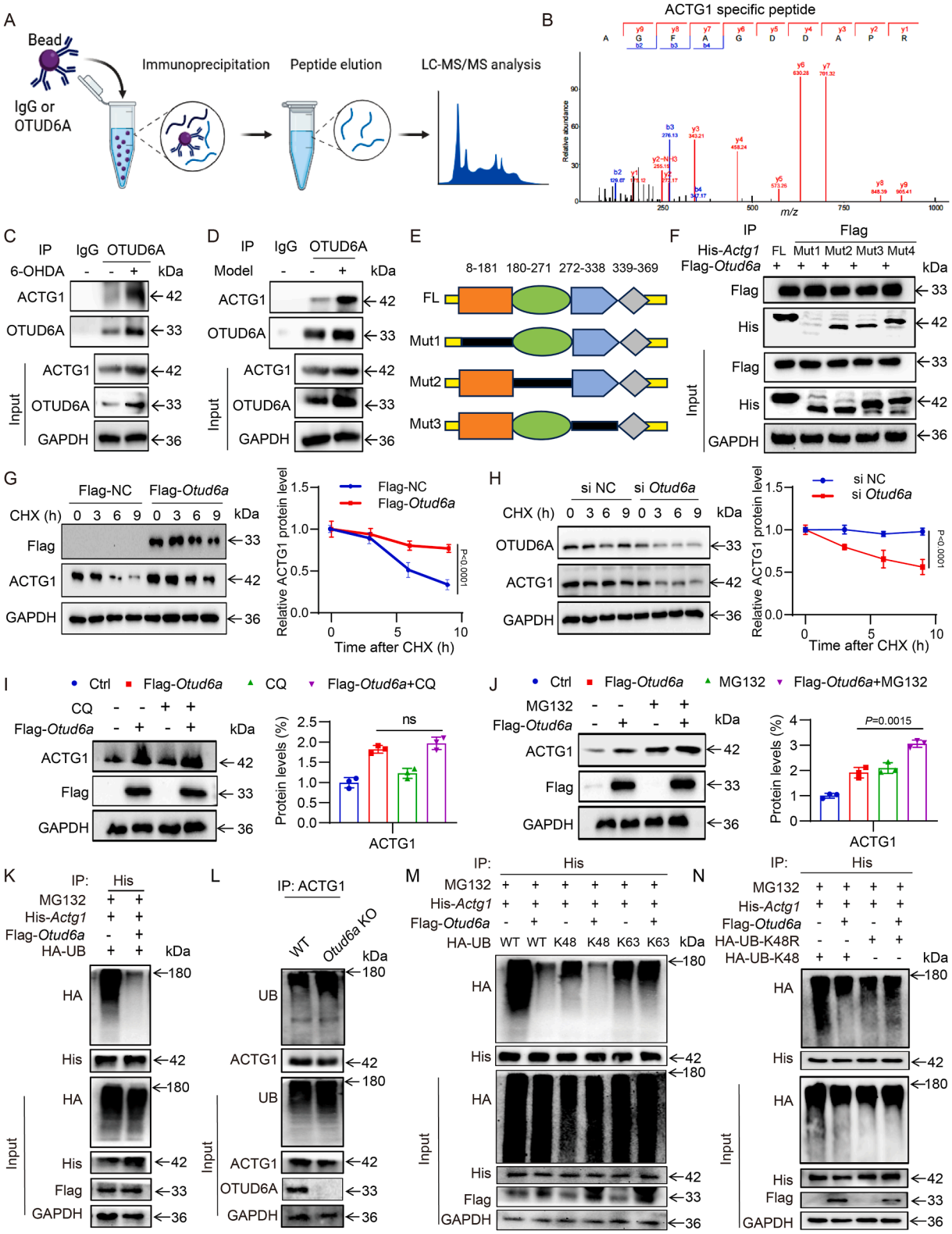

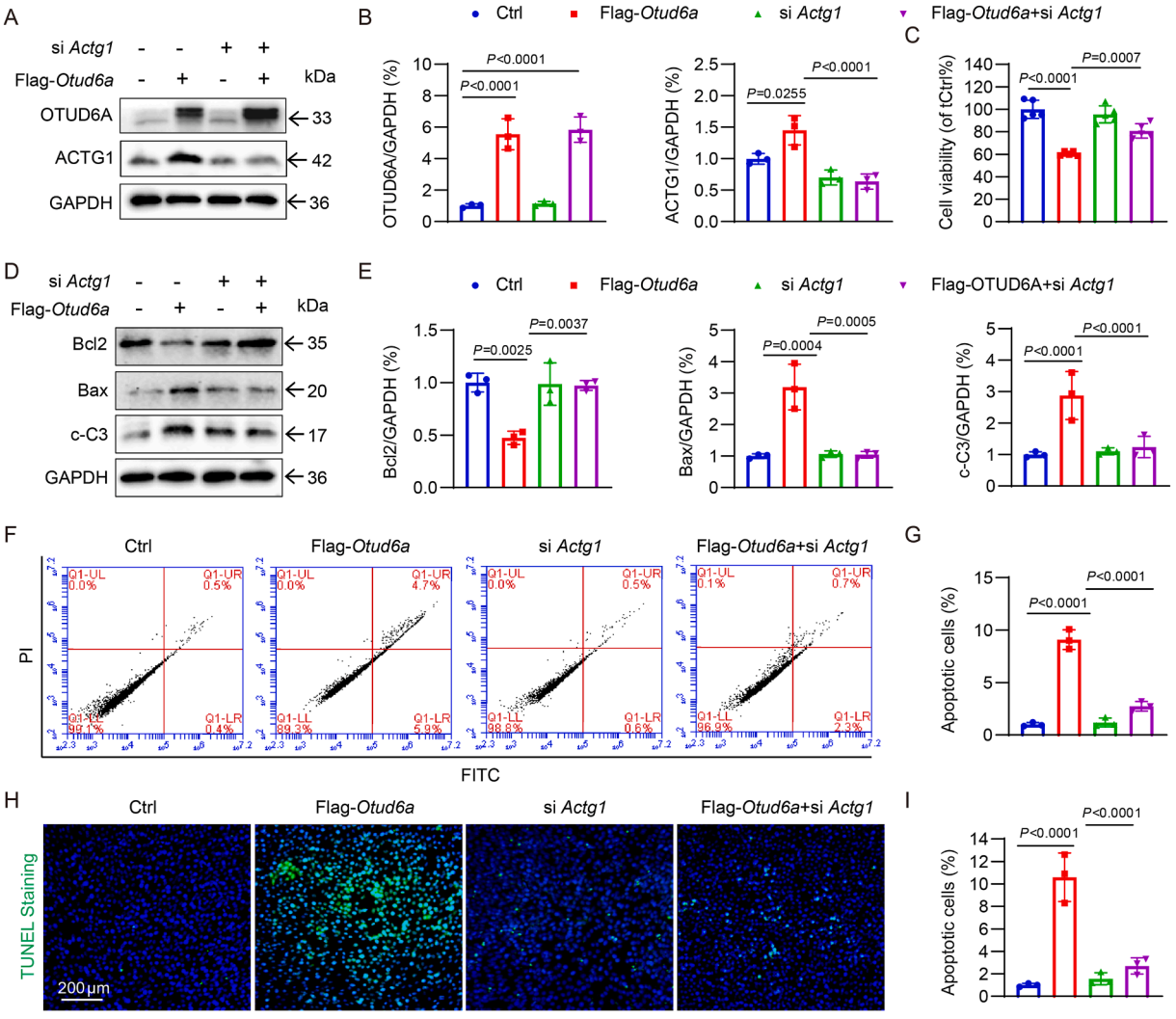

Figure 6 ACTG1 regulates the effect of OTUD6A on neuron apoptosis. (A) Western blot verification of *Otud6a* overexpression and *Actg1* knockdown efficiency in co-transfected PC12 cells. (B) Densitometric quantification of protein levels from panel (A) normalized to GAPDH. (C) Cell viability were measured by MTT assay ($n = 5$ duplicates/group). (D) Apoptotic protein profiling showing Bcl-2, Bax, and cleaved caspase-3 expression under indicated conditions. (E) Quantitative analysis of apoptosis-related proteins from panel (D) presented as Bcl-2/Bax ratio and cleaved caspase-3/GAPDH. (F, G) Flow cytometric analysis of apoptosis rates using Annexin V-FITC/PI staining: (F) representative plots and (G) quantification. (H, I) TUNEL assay demonstrating apoptotic nuclei: (H) representative images and (I) quantification of TUNEL-positive cells. (Mean ± SEM; $n = 3$ independent experiments).

Figure 5 OTUD6A **interact** with ACTG1 and regulates its stability through K48-linked deubiquitination. (A) Workflow schematic of LC−MS/MS analysis for identifying OTUD6A-interacting proteins. (B) Representative mass spectrum showing the identified ACTG1 peptide sequence. (C) Co-immunoprecipitation (Co-IP) analysis confirming OTUD6A−ACTG1 interaction in PC12 cell lysates. (D) Co-IP analysis of OTUD6A−ACTG1 interactions in the mouse substantia nigra. (E) Schematic diagram of the structure of ACTG1 and design of four different truncated fragment plasmids, all labeled with Flag. (F) Flag-OTUD6A and His-ACTG1FL, His-ACTG1Mut1, His-ACTG1Mut2, and His-ACTG1Mut3 plasmids were transferred to NIH3T3 cells. The binding regions of OTUD6A and ACTG1 were detected using Co-IP analysis. (G) Western blot to test the effects of *Otud6a* overexpression on ACTG1 stability. (H) Western blot to test the effects of *Otud6a* knockdown on ACTG1 stability. (I, J) Evaluation of degradation pathways using (I) autophagy inhibitor chloroquine (CQ, 20 μmol/L) or (J) proteasome inhibitor MG132 (10 μmol/L) in OTUD6A-modulated cells. (K) Ubiquitination assay showing reduced ACTG1 polyubiquitination upon *Otud6a* overexpression in NIH3T3 cells co-transfected with His-ACTG1, HA-ubiquitin (HA-UB), and Flag-OTUD6A. (L) Enhanced ACTG1 ubiquitination in substantia nigra tissue from *OTUD6A* knockout mice (immunoprecipitated with anti-ACTG1). (M) Ubiquitin linkage specificity assay demonstrating OTUD6A preferentially cleaves K48-linked chains (cells co-transfected with His-ACTG1, Flag-OTUD6A, and either HA-K48-UB or HA-K63-UB). (N) Validation of K48-specific regulation using ubiquitin mutant (K48R) in Co-IP assays. (Mean ± SEM; $n = 3$ independent experiments).

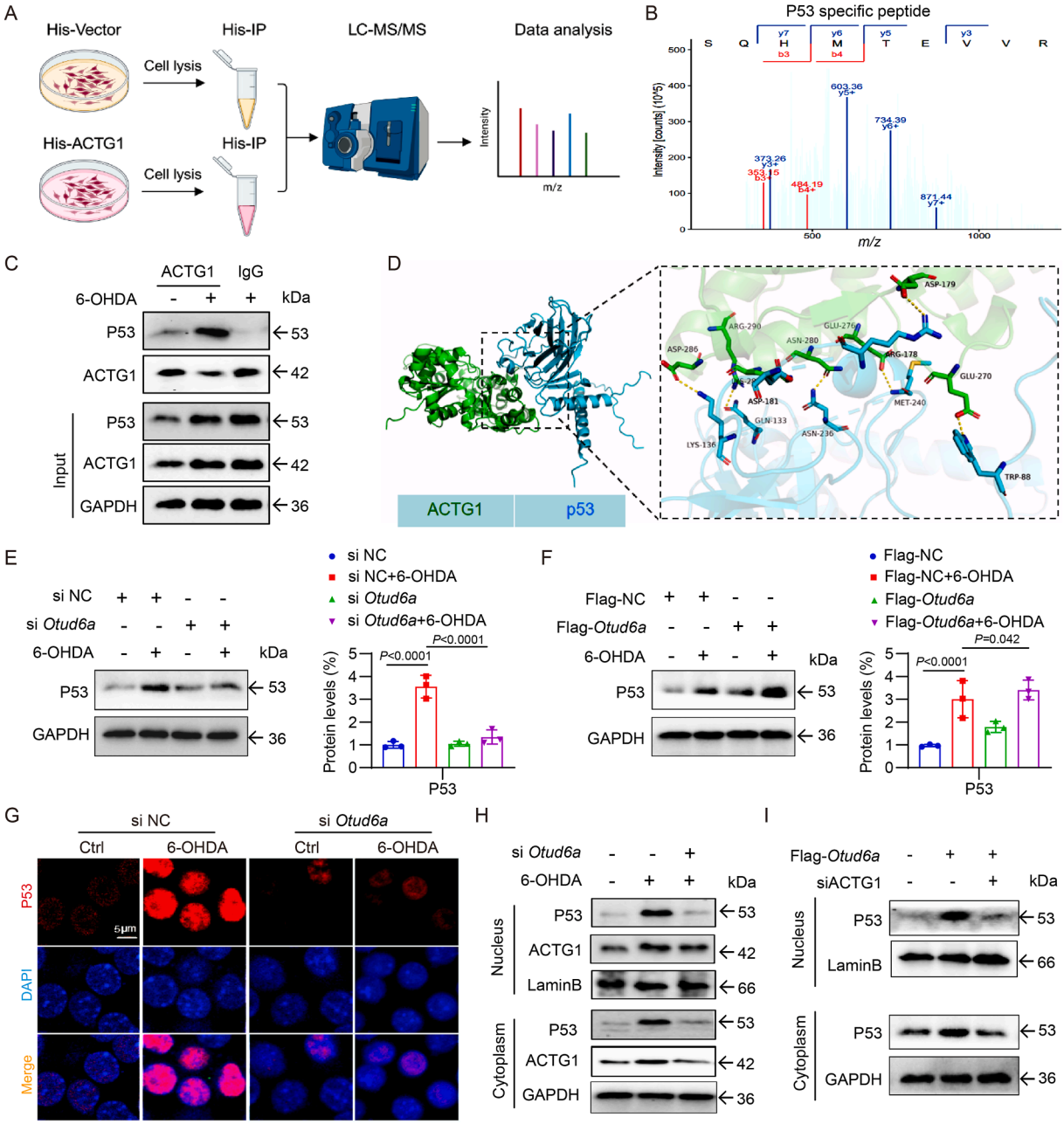

Figure 7 The OTUD6A−ACTG1 axis regulates p53-mediated apoptosis. (A)Workflow for mass spectrometry-based identification of ACTG1 interacting proteins. (B) LC−MS/MS analysis of potential ACTG1-binding partners in PC12 cell lysates. (C) Co-immunoprecipitation validation of ACTG1−p53 interaction *in vivo*. (D) Molecular docking simulation of ACTG1−p53 binding interface (presented as lowest energy conformation). (E) Western blot analysis of p53 expression after OTUD6A knockdown in PC12 cells. (F) Western blot analysis of p53 expression after OTUD6A overexpression. (G) Immunofluorescence staining of p53 (red) and DAPI (blue) showing subcellular localization following OTUD6A knockdown. (H) Nuclear fractionation assay quantifying p53 levels in nuclear extracts after OTUD6A knockdown. (I) Nuclear p53 accumulation under combined OTUD6A overexpression and ACTG1 knockdown. (Mean ± SEM; $n = 3$ independent experiments).

contribute to 6-OHDA induced neuronal death, suggesting that its dysregulation may be a key mechanism in dopaminergic injury[41]. A central finding of our study is the identification of p53 as a downstream effector of the OTUD6A−ACTG1 axis. p53 is a well-established regulator of cellular stress responses, and its activation has been observed in multiple PD models, including 6-OHDA treated neurons and postmortem patient brains[27]. Under neurodegenerative conditions, p53 promotes mitochondrial dysfunction, oxidative stress, and apoptosis processes central to PD progression[42-44]. These studies identify p53 as an essential modulator of dopaminergic neuronal integrity, influencing both survival and functional maintenance. We show that ACTG1 physically associates with p53 and facilitates its nuclear translocation, thereby amplifying the transcription of pro-apoptotic genes. This mechanism is consistent with prior evidence that ACTG1 can interact with p53 and influence neuronal survival[26,45]. Here, we

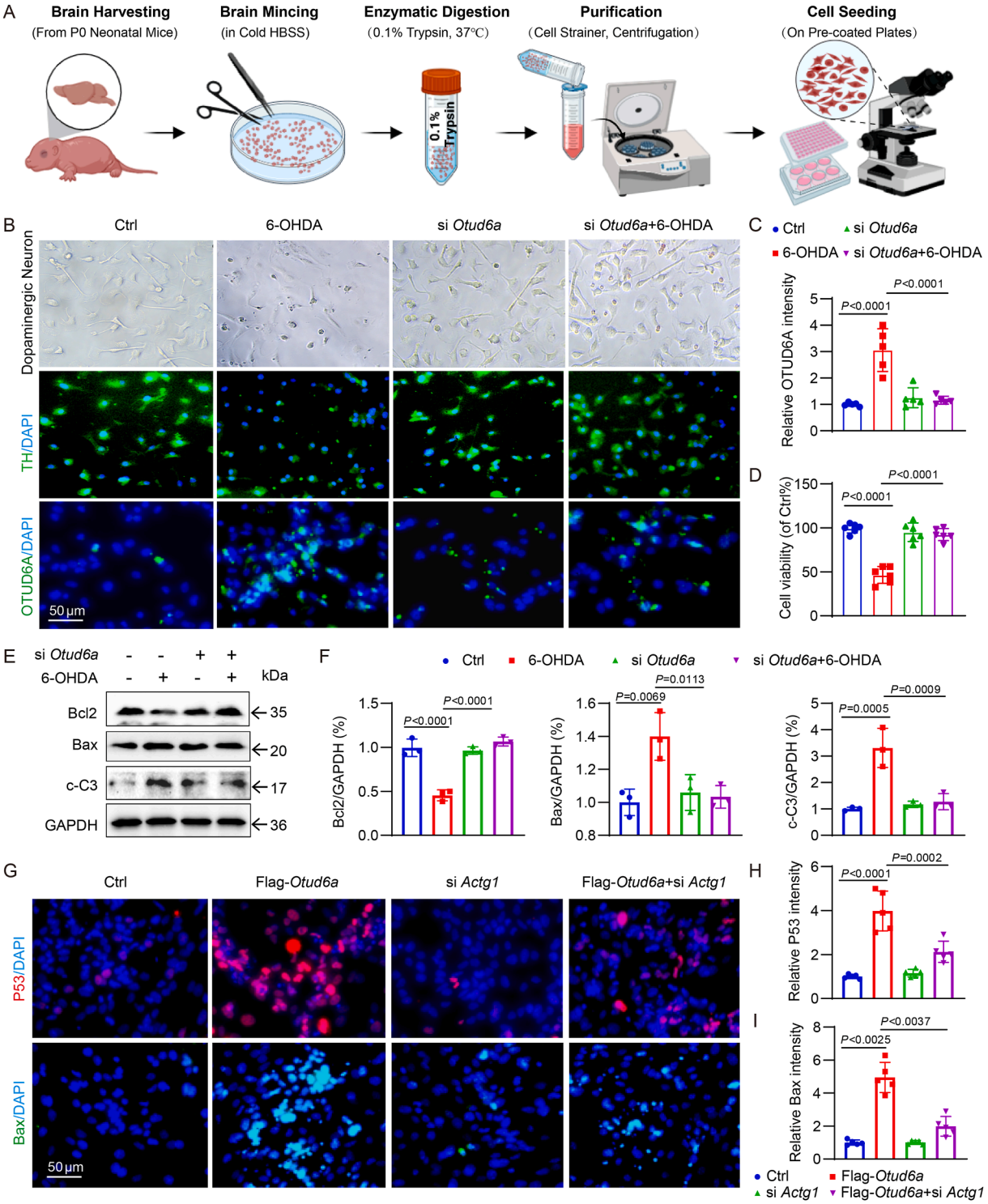

Figure 8 *Otud6a* deficiency attenuates 6-OHDA induced apoptosis in primary dopaminergic neurons *via* the ACTG1−p53 pathway. (A) Schematic of the primary ventral mesencephalic dopaminergic neuron culture protocol. (B) Phase-contrast image and immunofluorescence staining of TH (green) and OTUD6A (red) in primary dopaminergic neurons from each group. (C) Quantification of OTUD6A fluorescence intensity across groups. (D) Cell viability measured by MTT assay in primary dopaminergic neurons transfected with OTUD6A-targeting siRNA (si*Otud6a*) for 24 h and treated with 6-OHDA (100 μmol/L, 24 h). (E) Western blot analysis of Bcl2, Bax, and cleaved caspase-3 expression. (F) Quantification of protein levels from E. (G) Immunofluorescence staining of p53 and Bax in primary dopaminergic neurons under *Otud6a* overexpression and/or *Actg1* knockdown. (H) Quantification of p53 fluorescence intensity from (G). (I) Quantification of Bax fluorescence intensity from (G). (Mean ± SEM; $n = 3$ independent experiments).

demonstrate that (1) p53 functions as downstream of OTUD6A in this signaling pathway, and (2) ACTG1 physically associates with p53 to facilitate its nuclear translocation, thereby initiating the transcriptional program of neuronal apoptosis. Specifically, we investigated the effects of *Otud6a* knockdown and overexpression on p53 activation and neuronal apoptosis in primary mouse dopaminergic neurons. Together, these results delineate a linear signaling pathway in which OTUD6A stabilizes ACTG1, leading to p53 nuclear accumulation and transcriptional activation, ultimately driving dopaminergic degeneration in PD.

Current understanding of ubiquitination and deubiquitination mechanisms affecting ACTG1 and related actin isoforms primarily involves indirect regulatory pathways. These are often mediated through intermediate signaling molecules such as Rho GTPases, Src kinases, cofilin, and cortactin[46]. Several DUBs have been implicated in the modulation of actin dynamics: CYLD regulates Rac activation through RhoGTPase modulation, and USP22 influences actin polymerization *via* transcriptional control[46,47]. USP17 modulates Rho GTPase activity during cell migration[48]. Additionally, pharmacological inhibition of USP5, UCHL1, USP9X, USP14, and UCH37 has been shown to disrupt actin polymerization in leukemic cells through cofilin suppression, suggesting DUBs' involvement in actin-related pathologies[46]. Notably, direct regulatory mechanisms governing ACTG1 stability through ubiquitination or deubiquitination remain largely unexplored. To date, TRIM3 is the only E3 ubiquitin ligase known to promote ACTG1 degradation *via* the ubiquitin−proteasome pathway[49]. However, key mechanistic aspects. Such as the specific lysine residues targeted for ubiquitination and the topology of ubiquitin linkages involved have not been elucidated. Additionally, we cannot rule out potential contributions from other OTUD6A substrates in neural cell biology. In this study, we identify OTUD6A as the first DUB capable of directly stabilizing ACTG1 through deubiquitination, specifically by cleaving K48-linked polyubiquitin chains to prevent proteasomal degradation. This finding establishes a novel regulatory axis in actin dynamics and highlights OTUD6A's unique role in counteracting ACTG1 degradation. Despite this advance, the exact lysine residues (among ∼20 conserved lysine residues in ACTG1 protein) for OTUD6A-mediated deubiquitination remain a key question unresolved and need further exploration. Future studies should focus on the identification of these ubiquitination/deubiquitination sites to fully delineate the OTUD6A−ACTG1 regulatory axis in neuronal cells.

In summary, our findings reveal a previously unrecognized mechanism through which OTUD6A promotes neuronal apoptosis *via* deubiquitination of ACTG1 and subsequent activation of the ACTG1−p53 signaling pathway. This study identifies the OTUD6A−ACTG1−p53 axis as a promising therapeutic target for PD. Pharmacological inhibition of OTUD6A or modulation of this pathway may offer a novel neuroprotective strategy to mitigate dopaminergic neuron degeneration and slow disease progression in PD.

Acknowledgments

This study was supported by the National Natural Science Foundation of China (21961142009 to Guang Liang and 82501725 to Xia Zhao), Hangzhou Natural Science Foundation (2024SZRYBH090002to Xia Zhao), Medical and Health Science and Technology Project of Zhejiang Province (2025KY1032 to Xia Zhao). Also, we would like to thank the support from the Scientific Research Center, Hangzhou Medical College.

Author contributions

Guang Liang contributed to the literature search and study design. Xia Zhao participated in the drafting of the article. Guang Liang revised the manuscript. Xia Zhao, Fan Chen, Li Xiong, Xiaoxia Xu, Ziyao Meng, Luyao Li, Yu Deng and Qi Ai carried out the experiments. Qin Yu, Linjie Chen, Ruya Wang and Yiyu Ren contributed to data collection and analysis. Wenhua Zheng contributed to methodology. Jurui Wei and Houming Yu contribute to software and formal analysis. All authors read and approved the final manuscript.

Conflicts of interest

The authors declare no conflicts of interest.

Appendix A. Supporting information

Supporting information to this article can be found online at https://doi.org/10.1016/j.apsb.2025.12.002.

References

1. Rasheed MZ, Andrabi SS, Salman M, Tabassum H, Shaquiquzzaman M, Parveen S, et al. Melatonin improves behavioral and biochemical outcomes in a rotenone-induced rat model of Parkinson's disease. *J Environ Pathol Toxicol Oncol* 2018;**37**:139−50.
2. Luo B, Zhang H, Qin L. Case report: reversible encephalopathy caused by dyskinesia-hyperpyrexia syndrome. *Front Neurol* 2023;**14**:1234974.
3. Xie J, Chen S, Bopassa JC, Banerjee S. Drosophila tubulin polymerization promoting protein mutants reveal pathological correlates relevant to human Parkinson's disease. *Sci Rep* 2021;**11**:13614.
4. Herbers C, Schroeder J, Lu C, Geng H, Zhang R, Mehregan J, et al. Dopamine replacement therapy normalizes reactive step length to postural perturbations in Parkinson's disease. *Gait Posture* 2023;**101**:95−100.
5. You H, Mariani LL, Mangone G, Le Febvre de Nailly D, Charbonnier-Beaupel F, Corvol JC. Molecular basis of dopamine replacement therapy and its side effects in Parkinson's disease. *Cell Tissue Res* 2018;**373**:111−35.
6. Crosignani PG, Reschini E, Peracchi M, Lombroso GC, Mattei A, Caccamo A. Failure of dopamine infusion to suppress the plasma prolactin response to sulpiride in normal and hyperprolactinemic subjects. *J Clin Endocrinol Metab* 1977;**45**:841−4.
7. Guo J-J, Yue F, Song D-Y, Bousset L, Liang X, Tang J, et al. Intranasal administration of α-synuclein preformed fibrils triggers microglial iron deposition in the substantia nigra of Macaca fascicularis. *Cell Death Dis* 2021;**12**:81.
8. Tokunaga F, Ikeda F. Linear ubiquitination in immune and neurodegenerative diseases, and beyond. *Biochem Soc Trans* 2022;**50**:799−811.
9. Mi Z, Graham SH. Role of UCHL1 in the pathogenesis of neurodegenerative diseases and brain injury. *Ageing Res Rev* 2023;**86**:101856.
10. Hallengren J, Chen PC, Wilson SM. Neuronal ubiquitin homeostasis. *Cell Biochem Biophys* 2013;**67**:67−73.
11. Zheng N, Shabek N. Ubiquitin ligases: structure, function, and regulation. *Annu Rev Biochem* 2017;**86**:129−57.
12. Monaco A, Fraldi A. Protein aggregation and dysfunction of autophagy−lysosomal pathway: a vicious cycle in lysosomal storage diseases. *Front Mol Neurosci* 2020;**13**:37.
13. Fernández-Cruz I, Reynaud E. Proteasome subunits involved in neurodegenerative diseases. *Arch Med Res* 2021;**52**:1−14.
14. Zhao Q, Wang X, Zhang T, Guo S, Liu X, Wan S, et al. Piceatannol upregulates USP14-mediated GPX4 deubiquitination to inhibit

neuronal ferroptosis caused by cerebral ischemia−reperfusion in mice. *Food Chem Toxicol* 2025;**197**:115281.
15. Ganjam GK, Terpolilli NA, Diemert S, Eisenbach I, Hoffmann L, Reuther C, et al. Cylindromatosis mediates neuronal cell death *in vitro* and *in vivo*. *Cell Death differ* 2018;**25**:1394−407.
16. Wu S, Lin T, Xu Y. Polymorphic USP8 allele promotes Parkinson's disease by inducing the accumulation of α-synuclein through deubiquitination. *Cell Mol Life Sci* 2023;**80**:363.
17. Pan W, Wang Y, Bai X, Yin Y, Dai L, Zhou H, et al. Deubiquitinating enzyme USP30 negatively regulates mitophagy and accelerates myocardial cell senescence through antagonism of Parkin. *Cell Death Discov* 2021;**7**:187.
18. Kim SH, Baek KH. Ovarian tumor deubiquitinase 6A regulates cell proliferation *via* deubiquitination of nucleolin and caspase-7. *Int J Oncol* 2022;**61**.
19. Fu X, Zhao J, Yu G, Zhang X, Sun J, Li L, et al. OTUD6A promotes prostate tumorigenesis *via* deubiquitinating Brg1 and AR. *Commun Biol* 2022;**5**:182.
20. Zhao Y, Huang X, Zhu D, Wei M, Luo J, Yu S, et al. Deubiquitinase OTUD6A promotes breast cancer progression by increasing TopBP1 stability and rendering tumor cells resistant to DNA-damaging therapy. *Cell Death Differ* 2022;**29**:2531−44.
21. Sun J, Li H, Jin Y, Yu J, Mao S, Su KP, et al. Probiotic Clostridium butyricum ameliorated motor deficits in a mouse model of Parkinson's disease *via* gut microbiota−GLP-1 pathway. *Brain Behav Immun* 2021;**91**:703−15.
22. Goloborshcheva VV, Kucheryanu VG, Voronina NA, Teterina EV, Ustyugov AA, Morozov SG. Synuclein proteins in MPTP-induced death of substantia nigra pars compacta dopaminergic neurons. *Biomedicines* 2022;**10**:2278.
23. Yi LX, Tan EK, Zhou ZD. Tyrosine hydroxylase inhibitors and dopamine receptor agonists combination therapy for Parkinson's disease. *Int J Mol Sci* 2024;**25**:4643.
24. Wang H, Min J, Ding Y, Yu Z, Zhou Y, Wang S, et al. MBD3 promotes epithelial−mesenchymal transition in gastric cancer cells by upregulating ACTG1 *via* the PI3K/AKT pathway. *Biol Proced Online* 2024;**26**:1.
25. Luo JQ, Yang TW, Wu J, Lai HH, Zou LB, Chen WB, et al. Exosomal PGAM1 promotes prostate cancer angiogenesis and metastasis by interacting with ACTG1. *Cell Death Dis* 2023;**14**:502.
26. Torii T, Sugimoto W, Itoh K, Kinoshita N, Gessho M, Goto T, et al. Loss of p53 function promotes DNA damage-induced formation of nuclear actin filaments. *Cell Death Dis* 2023;**14**:766.
27. Kanapathipillai M. Treating p53 mutant aggregation-associated cancer. *Cancers(Basel)* 2018;**10**:154.
28. Kim TW, Koo SY, Riessland M, Chaudhry F, Kolisnyk B, Cho HS, et al. TNF−NF-κb−p53 axis restricts *in vivo* survival of hPSC-derived dopamine neurons. *Cell* 2024;**187**:3671−89.e23.
29. Bernstein AI, Garrison SP, Zambetti GP, O'Malley KLJMN. 6-OHDA generated ROS induces DNA damage and p53- and PUMA-dependent cell death. *Mol Neurodegener* 2011;**6**:2.
30. von Stockum S, Sanchez-Martinez A, Corrà S, Chakraborty J, Marchesan E, Locatello L, et al. Inhibition of the deubiquitinase USP8 corrects a Drosophila PINK1 model of mitochondria dysfunction. *Life Sci Alliance* 2019;**2**:e201900392.
31. Bingol B, Sheng M. Mechanisms of mitophagy: PINK1, Parkin, USP30 and beyond. *Free Radic Biol Med* 2016;**100**:210−22.
32. Jia F, Li H, Jiao Q, Li C, Fu L, Cui C, et al. Deubiquitylase OTUD3 prevents Parkinson's disease through stabilizing iron regulatory protein 2. *Cell Death Dis* 2022;**13**:418.
33. Shi L, Liu J, Peng Y, Zhang J, Dai X, Zhang S, et al. Deubiquitinase OTUD6A promotes proliferation of cancer cells *via* regulating Drp1 stability and mitochondrial fission. *Mol Oncol* 2020;**14**:3169−83.
34. Fang Z, Han J, Lin L, Ye B, Qu X, Zhang Y, et al. Deubiquitinase OTUD6a drives cardiac inflammation and hypertrophy by deubiquitination of STING. *Biochim Biophys Acta Mol Basis Dis* 2024;**1870**:167061.
35. Ren J, Yu P, Liu S, Li R, Niu X, Chen Y, et al. Deubiquitylating enzymes in cancer and immunity. *Adv Sci (Weinh)* 2023;**10**:e2303807.
36. Snyder NA, Silva GM. Deubiquitinating enzymes (DUBs): regulation, homeostasis, and oxidative stress response. *J Biol Chem* 2021;**297**:101077.
37. Li N, Zhou Y, Cai J, Wang Y, Zhou X, Hu M, et al. A novel trans-acting lncRNA of ACTG1 that induces the remodeling of ovarian follicles. *Int J Biol Macromol* 2023;**242**:125170.
38. Yan Y, Xu H, Zhang L, Zhou X, Qian X, Zhou J, et al. RRAD suppresses the Warburg effect by downregulating ACTG1 in hepatocellular carcinoma. *OncoTargets Ther* 2019;**12**:1691−703.
39. Wu T, Jia X, Feng H, Wu D. ACTG1 regulates intervertebral disc degeneration *via* the NF-κB−p65 and Akt pathways. *Biochem Biophys Res Commun* 2021;**545**:54−61.
40. Zhou C, Jiang X, Liang A, Zhu R, Yang Y, Zhong L, et al. COX10-AS1 facilitates cell proliferation and inhibits cell apoptosis in glioblastoma cells at post-transcription level. *Neurochem Res* 2020;**45**:2196−203.
41. Liu J, Liu H, Zhao Z, Wang J, Guo D, Liu Y. Regulation of Actg1 and Gsta2 is possible mechanism by which capsaicin alleviates apoptosis in cell model of 6-OHDA-induced Parkinson's disease. *Biosci Rep* 2020;**40**:BSR20191796.
42. Luo Q, Sun W, Wang YF, Li J, Li DW. *Association of p53 with neurodegeneration in Parkinson's disease*, vol 2022. Parkinsons Dis; 2022. p. 6600944.
43. Gomez-Lazaro M, Galindo MF, Concannon CG, Segura MF, Fernandez-Gomez FJ, Llecha N, et al. 6-Hydroxydopamine activates the mitochondrial apoptosis pathway through p38 MAPK-mediated, p53-independent activation of Bax and PUMA. *J Neurochem* 2008;**104**:1599−612.
44. Song Y. Identifying p53-independent apoptosis. *Nat Chem Biol* 2024;**20**:796.
45. Wang L, Wang M, Wang S, Qi T, Guo L, Li J, et al. Actin polymerization negatively regulates p53 function by impairing its nuclear import in response to DNA damage. *PLoS One* 2013;**8**:e60179.
46. Xue Y, Xue C, Song W. Emerging roles of deubiquitinating enzymes in actin cytoskeleton and tumor metastasis. *Cell Oncol* 2024;**47**:1071−89.
47. Yang Y, Sun L, Tala Gao J, Li D, Zhou J, Liu M. CYLD regulates RhoA activity by modulating LARG ubiquitination. *PLoS One* 2013;**8**:e55833.
48. de la Vega M, Kelvin AA, Dunican DJ, McFarlane C, Burrows JF, Jaworski J, et al. The deubiquitinating enzyme USP17 is essential for GTPase subcellular localization and cell motility. *Nat Commun* 2011;**2**:259.
49. Schreiber J, Végh MJ, Dawitz J, Kroon T, Loos M, Labonté D, et al. Ubiquitin ligase TRIM3 controls hippocampal plasticity and learning by regulating synaptic γ-actin levels. *J Cell Biol* 2015;**211**:569−86.